 doi:10.20944/preprints202106.0601.v1

Original Article

Biocompatibility and antibacterial properties of TiCu(Ag) thin films produced by physical vapor deposition magnetron sputtering

Saqib Rashid[a,#], Gian Marco Vita[b,#], Luca Persichetti[b], Giovanna Iucci[b], Chiara Battocchio[b], Rostislav Daniel[c], Daniela Visaggio[b], Martina Marsotto[b], Paolo Visca[b], Edoardo Bemporad[a], Paolo Ascenzi[b,d], Giovanni Capellini[b], Marco Sebastiani[a*], Alessandra di Masi[b*]

[a]*Università degli Studi Roma Tre, Engineering Department, via della Vasca Navale 79, 00146 Rome, Italy*

[b]*Università degli Studi Roma Tre, Department of Science, Viale Guglielmo Marconi, 446, 00146 Rome, Italy*

[c]*Department of Materials Science, Montanuniversität Leoben, Franz-Josef-Straße 18, Leoben, 8700, Austria*

[d]*Accademia Nazionale dei Lincei, Via della Lungara 10, 00165 Rome, Italy*

# These Authors contributed equally to this work

Running title: Biocompatibility and antibacterial properties of TiCu(Ag) thin films

***Corresponding authors:**

Marco Sebastiani, e-mail: marco.sebastiani@uniroma3.it

Alessandra di Masi, e-mail: alessandra.dimasi@uniroma3.it

 doi:10.20944/preprints202106.0601.v1

Abstract

Mechanical robustness, biocompatibility, and antibacterial performances are key features for materials suitable to be used in tissue engineering applications. In this work, we investigated the link existing between structural and functional properties of TiCu(Ag) thin films deposited by physical vapor deposition magnetron sputtering on Si substrates. The thin films were characterized by X-ray diffraction (XRD), nanoindentation, atomic force microscopy (AFM), and X-ray photoelectron spectroscopy (XPS). The TiCu(Ag) thin films showed complete amorphous structure and improved mechanical properties in comparison with pure Ti films. However, for contents in excess of 20% Ag, we observed the appearance of nanometric Ag crystallite. The TiCu(Ag) thin films displayed excellent biocompatibility properties, allowing adhesion and proliferation of the human fibroblasts MRC-5 cell line. Moreover, all the investigated TiCu(Ag) alloy display bactericidal properties, preventing the growth of both *Pseudomonas aeruginosa* and *Staphylococcus aureus*. Results obtained from biological tests have been correlated to the surface structure and microstructure of films. The excellent biocompatibility and bactericidal properties of these multifunctional thin films opens to their use in tissue engineering applications.

Keywords: bactericidal; biocompatibility; copper; human fibroblast; physical vapor deposition (PVD); silver; titanium; thin films.

 doi:10.20944/preprints202106.0601.v1

1. Introduction

The aging of world population drives an increasing demand of tissue and organ replacements [1]. To date, more than 10 million transplantations are performed annually, with an yearly increase of about 6%, and an overall cost of more than $500 billion per year [2]. However, tissue and organ transplantations present two major limitations: the low availability of donors and/or risk of disease transmission and immune rejection [3-5].

Tissue engineering (TE) is an emerging and promising alternative approach of biomedicine to treat or to replace damaged tissues and organs. TE combines materials science, chemistry, physics, and cell biology to allow tissue and organ repair or reconstruction. TE is often based on nanoscaffolds enabling cell adhesion, migration, proliferation, and differentiation [6-9]. The properties of a scaffold mainly depend upon the types of biomaterial and fabrication techniques [8]. In particular, the size, the shape, and patterning of adhesion sites are crucial elements in the design of effective scaffold surfaces. Nano-scaffolds must be biocompatible and can be combined with organic and inorganic materials to mimic the structure and function of the natural extracellular matrix (ECM). The ECM allows the cells to accomplish the biochemical and biophysical functions related to tissue and/or organs regeneration [8, 10]. Cells grown on nanoscaffolds can generate biocompatible, immunocompatible, and biofunctional tissues inside the body, counteracting the drawbacks associated with autologous grafting and allograft tissue transplantation, thereby alleviating the risk of rejection [8-9].

Another critical issue of nanoscaffolds is their capability to prevent microbial growth. Antimicrobial capability is conventionally obtained by means of biochemical approaches relying on nanoscaffold coating with biocidal substances such as silver and antibiotics. Nonetheless, chemical toxicity, antimicrobial durability, and microbial resistance remain critical problems [11].

 doi:10.20944/preprints202106.0601.v1

In this complex framework, surface engineering and the development of nanostructured thin films is gaining importance, especially for applications where a combination among surface hardness (or wear resistance), biocompatibility, and antibacterial performance are desired. Recently, multi-element thin films, such as Zr-based thin films (*e.g.*, Zr-Cu, Zr-Cu-Ag, ZrCN, Zr/ZrCN multilayer) [12, 13] and Ti-based thin films (*e.g.*, TiN, TiCu, Ti-Zr-Si) have emerged as a new class of nano-engineered thin films, featuring an excellent combination of high mechanical strength and biocompatibility. Moreover, these films are promising systems for biocompatible coating deposition. Indeed, the use of physical vapor deposition (PVD) for their growth allows a fine control of the material nanostructure, which leads to increased hardness and wear resistance [14, 15]. The desired combination of mechanical strength, biocompatibility, and antimicrobial activity can also be achieved by constructing multi-layers. Recent studies have confirmed the potential antibacterial behavior of Au, Cu, Zn, Ag additions to Ti-based films [16, 17]. The biocidal performance of Cu is linked to the release of Cu^{+1} and Cu^{+2} ions, as observed in TiCu [18, 19]. Recently, Cu-based systems have also been proposed engineer surfaces with antiviral properties, also in the framework of the COVID-19 pandemic [20]. Very recent examples include Cu-coated touch surface fabricated by cold-spray technology, as well as antiviral Cu_xO/TiO_2 photo catalyst thin films with photo-activated anti-viral properties [21, 22]. Consequently, the TiCu systems are of particular interest for the generation of material systems, featuring both anti-infective properties and surface hardness, as required in human implants and/or touch surfaces [23, 24].

In this context, the development of antibacterial metallic thin films combining biocompatibility with relatively high surface hardness, as witnessed by the growth of human fibroblasts, is here reported. To this aim, in this work we investigate TiCu(Ag) PVD sputtered thin films to evaluate their potential as biomedical thin films. By using high-resolution surface chemical and morphological characterization combined with cell growth studies and

Preprints (www.preprints.org) | NOT PEER-REVIEWED | Posted: 24 June 2021 doi:10.20944/preprints202106.0601.v1

antibacterial tests, significant biocompatibility and antibacterial properties have been observed, and correlated to film structure and surface properties.

2. Materials and methods

2.1. Thin film deposition

TiCu(Ag) thin films were deposited on 21×7 mm^2 coupons extracted from 4" Si(001) undoped wafers by means of direct current (DC) magnetron sputtering in a deposition system equipped with three unbalanced magnetrons. For the deposition, we have used Ti, Cu, and Ag targets with a 3" diameter and 99.99% purity were employed. The Si substrates were cleaned in ultrasonic bath and ethanol for 10 minutes before mounting them on the substrate holder. An Ar^+ sputtering step (powered by radio frequency (RF) power supply at 50 KHz, at the Ar pressure of 1.2 Pa and a discharge power of 0.03 KW) was performed to clean and activate the Si surface immediately prior to metal deposition. The distance between the substrates and targets was 70 mm, while the substrate was kept in rotation at 80 rpm. All the depositions were performed at a 0.52 Pa Ar pressure (chamber base vacuum of 1.0×10^{-5} Pa), with no intentional substrate heating. By applying different DC-power to the targets for 40 min, 4 sample sets were obtained, always keeping the Ti:Cu ratio equal to ~1. Deposition conditions, thickness, and composition are listed in Table 1.

Table 1. Composition of the TiCu(Ag) thin films.

Film composition	Ti:Cu ~ 1	Power at Ti (W)	Power at Ti (W)	Power at Ti (W)	Thickness of the film (µm)
TiCu	48:52	150	29	0	1.48
TiCu-10% Ag	43:47	143	27	3	1.44
TiCu-20% Ag	38:42	128	24	5	1.43
TiCu-30% Ag	33:37	113	21	9	1.46

Preprints (www.preprints.org) | NOT PEER-REVIEWED | Posted: 24 June 2021 doi:10.20944/preprints202106.0601.v1

2.2. *Characterization of thin films*

Crystallographic structure of the thin films was carried out by X-ray diffraction (XRD), using a θ-2θ Bruker D8 Advanced system with Cu Kα radiation (λ = 0.154 nm). Diffraction scans were performed by using grazing incident angle of 0.75 degree with time step of 0.02˚/sec. The chemical composition of the thin films was estimated via energy dispersive X-ray spectroscopy (EDX, Oxford instrument INCA), using built-in sensitivity factors for calibration. The film thickness was measured by using a white light optical profilometer with a Leica DCM 3D software package via automatic step measurement of the coated and the uncoated parts of the substrate.

The elastic modulus (E) and hardness (H) values were determined using nano-indentation testing method using a KLA-Nanomechanics G200 fitted with a Berkovich diamond indenter operating in continuous stiffness measurement mode, hence allowing obtaining both E and H as a continuous function of the depth from a single indentation experiment [25]. A standard fused silica sample was tested before and after a batch of measurements to calibrate the tip, so to ensure the reliability of the results. A least 25 indentations were performed on each sample. Calculations were made by the Oliver and Pharr method from the load-displacement curve using 10% of the film thickness at the maximum indentation depth [26].

2.3. *X-ray Photoelectron Spectroscopy (SR-XPS)*

X-ray Photoelectron Spectroscopy (SR-XPS) measurements were performed at the materials science beamline (MSB) of the Elettra synchrotron radiation source (Trieste, Italy). The UHV end station, with a base pressure of 2×10^{-10} mbar, is equipped with a SPECS PHOIBOS 150 hemispherical electron analyzer and a dual-anode Mg/Al X-ray source, an ion gun, and a sample manipulator with a K-type thermocouple attached to the rear side of the

Preprints (www.preprints.org) | NOT PEER-REVIEWED | Posted: 24 June 2021 doi:10.20944/preprints202106.0601.v1

sample. Al Kα radiation at 1486.6 eV photon energy impinging at 60° was used to analyze the Cu2p, Ti2p, Ag3d, C1s, N1s and O1s core levels on the respective samples. Photoelectrons were detected at normal emission geometry.

Calibration of the energy scale was made referencing the spectra to the C1s core level signal of aliphatic C atoms (285.0 eV). Curve-fitting analysis of the experimental spectra was carried out using Gaussian curves as fitting functions. The $Ti2p_{3/2,1/2}$ core level were fitted using a spin−orbit splitting of 5.7 eV and a branching ratio ($2p_{3/2}/2p_{1/2}$) of 2; the $Cu2p_{3/2,1/2}$ doublets were fitted using a spin-orbit splitting of 19.8 eV and a branching ratio ($2p_{3/2}/2p_{1/2}$) of 2. For the $Ag3d_{5/2,3/2}$ doublets, a splitting of 6.0 eV and a branch $3d_{5/2}/3d_{3/2}$ ratio of 3/2 were used. When different species were identified in a spectrum, the same Full Width at Half Maximum (FWHM) value was set for all individual photoemission peaks. Atomic ratios were calculated from peak intensities by using Scofield's cross section values.

2.4. Surface sterilization

Thin films were rinsed in 70% ethanol in sterile deionized water and then flamed with a Bunsen burner. Sterilization was performed under biosafety cabinets with installed HEPA filters to avoid contamination. After sterilization, films were air-dried, and structural and mechanical properties were evaluated in order to verify stability prior to testing for biocompatibility and antibacterial properties.

2.5. Human cells culture

MRC-5 human lung fibroblasts were cultured in Dulbecco's Modified Eagle Medium (DMEM) (Corning, VA, USA) complemented with 10% fetal bovine serum (FBS) (BioWest, Nuaillé, France), 100 mg/mL penicillin and streptomycin (Merck KGaA, Darmstadt, Germany), and 2.0×10^{-3} M L-glutamine (Merck KGaA). Cells were grown at 37°C and 5%

Preprints (www.preprints.org) | NOT PEER-REVIEWED | Posted: 24 June 2021 doi:10.20944/preprints202106.0601.v1

CO_2. Before seeding, cells were counted using the BLAUBRAND® counting chamber (Brand GMBH, Wertheim, Germany).

2.6. Evaluation of surfaces biocompatibility

To correlate MRC-5 cell density to the relative luminescence units (RLU) value, a calibration curve was set up. With this aim, MRC-5 cells were plated in triplicate in opaque 96-well plates at a density of 2.5×10^3, 5.0×10^3, 1.0×10^4, 2.0×10^4, and 4.0×10^4 cells/well. On the basis of the results obtained from the calibration curve, 1.0×10^4 MRC-5 fibroblasts were seeded on sterile TiCu surfaces coated with 0%, 10%, 20%, and 30% Ag thin films placed into opaque 96-well plates. Cell growth and proliferation was assessed by incubating MRC-5 fibroblasts for 10 min with the CellTiter-Glo® Luminescent reagent (Promega, Madison, WI, USA) added in a 1:1 ratio with the complete cell culture medium. Luminescence was measured using the Tecan Spark 10M plate reader (Tecan, Männedorf, Switzerland). Background luminescence was measured in the complete culture medium without cells, and subtracted from each experimental value.

2.7. Testing of the antibacterial properties

Bacteria were routinely grown in Nutrient Broth (NB) No. 2 (# CM0067B; Thermo Scientific™, Waltham, Massachusetts, USA). The day before the experiment, glycerol stocks of *S. aureus* ATCC 25923 or *P. aeruginosa* ATCC 15692 (strain PAO1) were streaked on NB supplemented with 15% agar (NA) plates and incubated at 37 °C for 24 h. By using sterile inoculating loops, bacterial colonies were transferred in 1 mL NB diluted 1:500 ($NB_{1:500}$) in deionized sterile water and the bacterial concentrations was adjusted to ~5.0×10^7 colony forming unit (CFU)/mL.

Preprints (www.preprints.org) | NOT PEER-REVIEWED | Posted: 24 June 2021 doi:10.20944/preprints202106.0601.v1

The plate count method was conducted according to a minor modification of the International Standard ISO 22196 protocol [27]. Briefly, each sterilized TiCu and TiCu(Ag) surface, as well as the glass control surface, was placed into a Petri dish (⌀ 3 cm). Then, 0.005 mL of a suspension of either *S. aureus* or *P. aeruginosa* at a concentration of ~ 5.0×10^7 colony forming unit (CFU)/mL was dripped onto the surfaces and samples were incubated at 37 °C overnight (ON) at 99% relative humidity. After incubation, each surface was placed into 1 mL $NB_{1:500}$ at room temperature for 15 min, and then vortexed for 1 min to allow the detachment of bacteria from the surface. The bacterial suspension was appropriately diluted and plated on NA for CFU counts. To determine the CFU at time 0 h, suspensions of either *S. aureus* or *P. aeruginosa* (presumptive concentration ~5.0×10^7 CFU/mL) were appropriately diluted in saline and plated onto NA. At least two samples were assessed for each bacterial strain. The antibacterial activity (BA) was calculated by the following formula:

$$BA = [(N_{0\,h} - N_{24\,h}) / N_0] \times 100\%$$

Where, $N_{0\,h}$ and $N_{24\,h}$ are the CFU average numbers counted at 0 h and 24 h, respectively, for each type of surface.

An agar diffusion assay was performed to detect the release of bacterial growth inhibitors. A suspension of either *S. aureus* or *P. aeruginosa* (OD_{600} = 0.1) was uniformly spread onto NA plates using a sterile cotton swab. TiCu and TiCu(Ag) surfaces were placed on the NA inoculated plates. The glass surface was used as negative control, whereas antibiotic discs (*i.e.*, erythromycin, E 15 µg; and amikacin, AK 30 µg) were used as positive control of bacterial inhibition. After 16-h incubation at 37 °C, the release of antibacterial factors by TiCu(Ag), glass surfaces, and antibiotic discs was visually assessed by the presence of the inhibition zone around the sample.

Preprints (www.preprints.org) | NOT PEER-REVIEWED | Posted: 24 June 2021 doi:10.20944/preprints202106.0601.v1

2.8. Morphological characterization

The surfaces were morphologically characterized by AFM and optical microscopy; the results obtained were compared to control samples represented by a suspension of bacteria poured directly on the TiCu surface. AFM measurements were performed using a Dimension ICON AFM (Bruker, Santa Barbara, CA) operating in peak-force mode. The AFM was equipped with a ScanAsyst-Air Bruker silicon probe featuring a nominal cantilever elastic constant of 0.4 N m^{-1} and a tip with a nominal radius of 2 nm. The oscillation frequency and oscillation amplitude of the cantilever were set to 1 kHz and 150 nm, respectively. For each measurement, height sensor and peak force error images were recorded simultaneously. The AFM images were analyzed and processed with the software Gwyddion [28], applying a first-order flattening. Surface roughness was obtained by measuring the root-mean-square deviation of surface heights on 20×20 μm^2 images. Optical microscopy images were acquired using a Nikon Eclipse ME600 microscope equipped with Nikon DXM1200 digital camera (Nikon, Tokio, Japan).

3. Results

3.1. Structural, morphological, chemical, and mechanical characterization of substrates

The X-ray diffraction patterns of the as-deposited thin films (see Table 1) are shown in Figure 1. The diffraction pattern of the TiCu(Ag) samples shows only a broad band in the [38-45˚] 2θ-range, pointing to an amorphous structure [29-30].

Preprints (www.preprints.org) | NOT PEER-REVIEWED | Posted: 24 June 2021 doi:10.20944/preprints202106.0601.v1

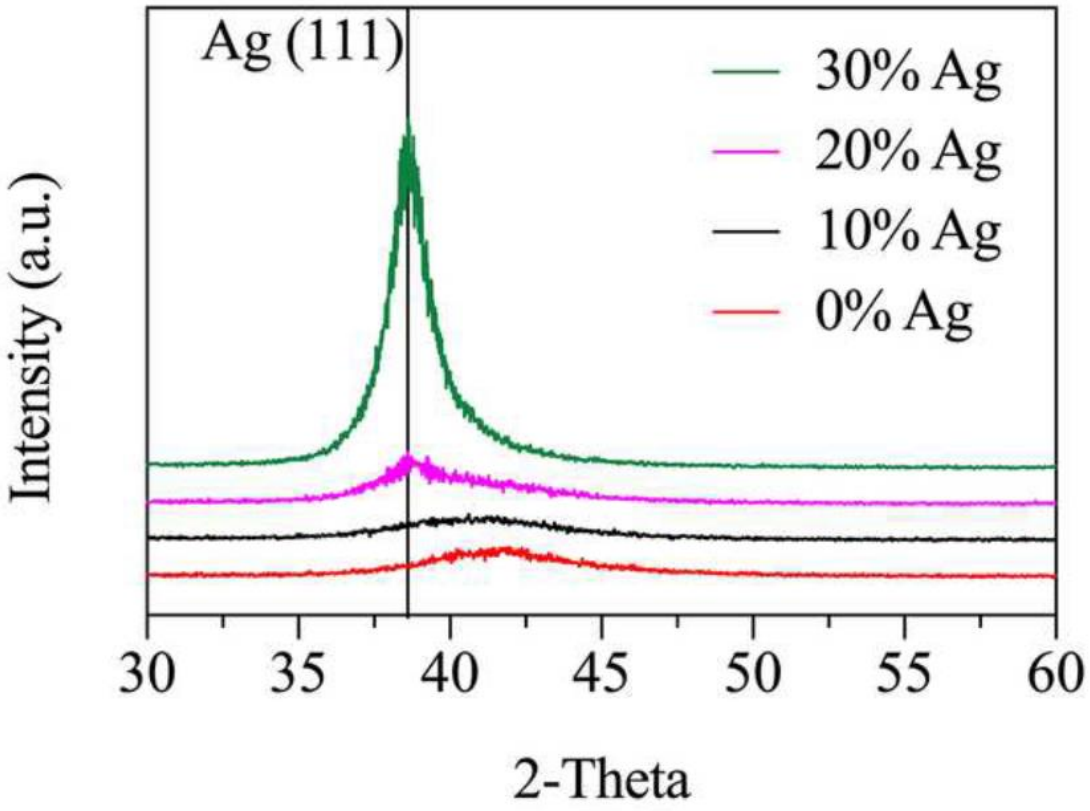

Figure 1. **X-ray diffraction pattern**. Diffraction scans of the TiCu and TiCu(Ag) thin films.

Preprints (www.preprints.org) | NOT PEER-REVIEWED | Posted: 24 June 2021 doi:10.20944/preprints202106.0601.v1

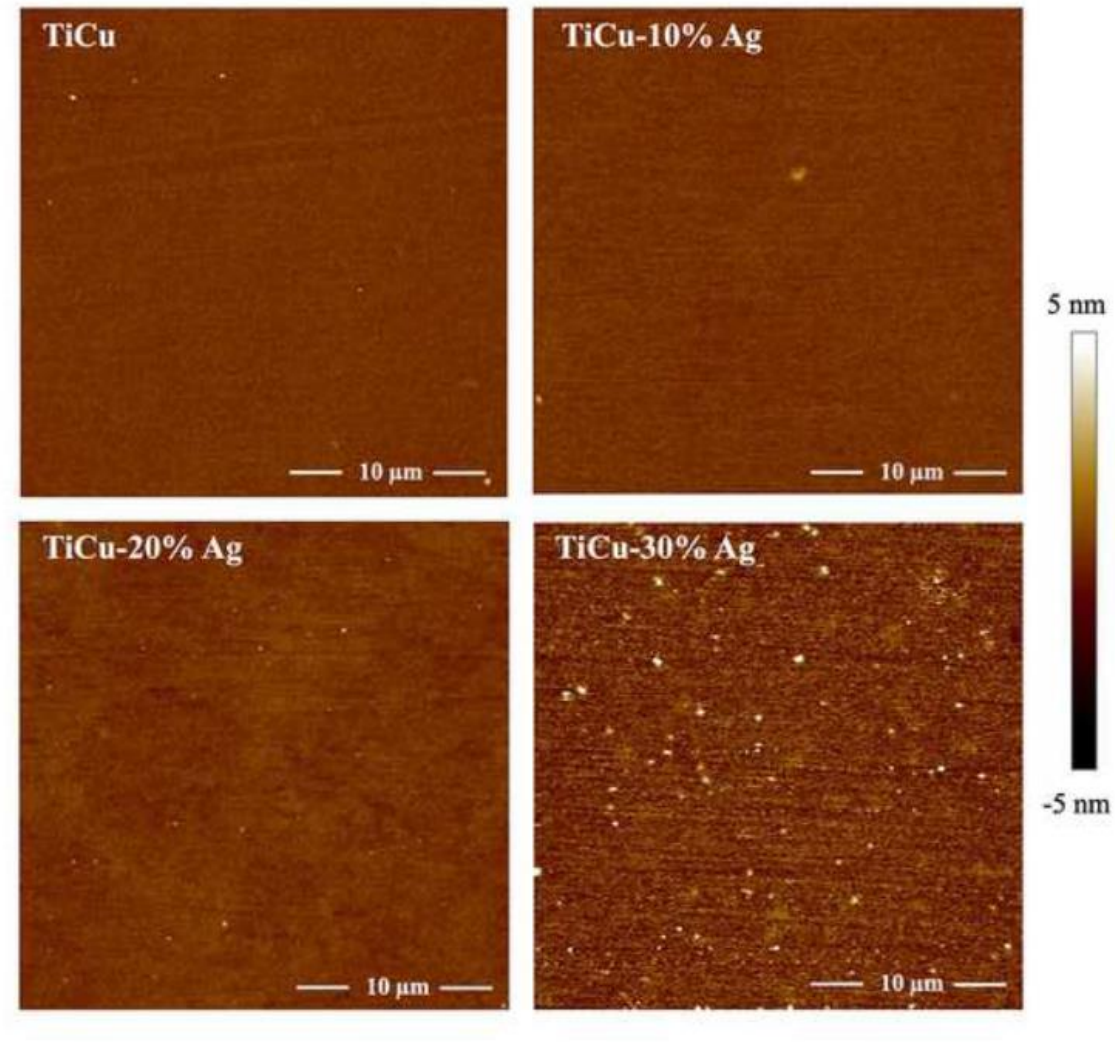

Figure 2. Characterization of the surface morphology. Atomic force microscopy (AFM) images of the TiCu and TiCu(Ag) thin films with an Ag content of 10%, 20%, and 30%.

For Ag concentration exceeding 10% , we observed the appearance of a second feature, whose angular potition is compatible with the Ag(111) reflection, showing an increasing intensity and a narrowing for increasing Ag contet. This point out to a Ag precipitation phenomenon with the formation of Ag nanocrystallites at Ag contents > 20%. By using the Scherrer's equation on XRD spectra, an Ag crystallite size of the order of 3-5 nm for the film with 20% Ag addition was estimated.

No impact on the XRD spectra has been observed flaming with alcohol.

 doi:10.20944/preprints202106.0601.v1

The AFM analysis revealed crack-free smooth surfaces for all thin films with an increase in the average roughness as the Ag content increased from 10 to 30%. The amorphous TiCu and TiCu(Ag) thin films with the Ag content below 20% exhibited an average surface roughness well below 0.5 nm. For TiCu(Ag) film featuring Ag content > 20%, we observed the appearance of nanocrystallites, which, in agreement with the XRD evidence above discussed, was attributed to the formation og Ag precipitates. Consequently, the surface roughness increases up to ~ 1 nm in the Ag-richest sample (see Fig. 3). It is worth noting that the surface clusters observed by AFM have a size larger than that obtained by the XRD analysis. This is not in contrast with our hypothesis, since the surface cluster might be formed by the assembly of different nanocrystallites of a lesser size.

Preprints (www.preprints.org) | NOT PEER-REVIEWED | Posted: 24 June 2021 doi:10.20944/preprints202106.0601.v1

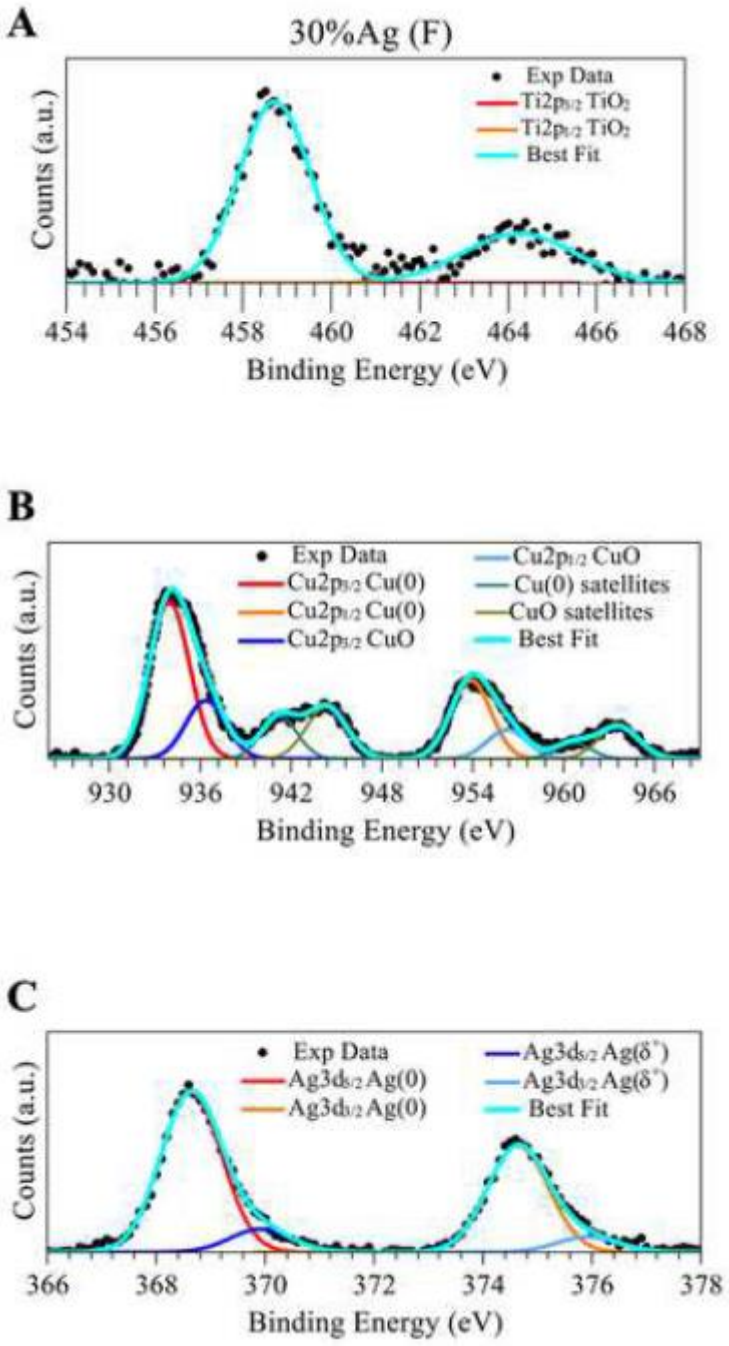

Figure 3. XPS spectra. (A) Ti2p, (B) Cu2p, and (C) Ag3d core level spectra of sample TiCu-30%Ag and related peak fitting analysis.

Thin films with such a low average surface roughness are in general very favorable for antibacterial and biomedical applications [31], especially if antimicrobial agents such as Cu and Ag are added into the protective thin film, which induce a release of metallic ions after exposure to a humid environment [32]. The elastic modulus E and hardness H of thin films

Preprints (www.preprints.org) | NOT PEER-REVIEWED | Posted: 24 June 2021 doi:10.20944/preprints202106.0601.v1

were calculated as a function of Ag contents by the nanoindentation method. The TiCu film exhibited the highest E = 124.3 GPa and H = 7.83 GPa values. As we can observe in Fig. 3 (left axis), the addition of Ag into the TiCu(Ag) thin films induced a decrease of both modulus and hardness, with the lowest values of modulus (109.25 GPa) and hardness (6.45 GPa) observed in the sample containing 30% of Ag.

After the flame sterilization test, no change was observed in the mechanical properties of thin film, consistent with a previous report [33]. All the samples were analyzed by XPS spectroscopy before and after flaming with alcohol (flamed samples will be labelled (F) in the following text). The measured binding energies (BE, ±0.2 eV), Full Width at Half Maximum, and atomic ratios calculated from peak areas for all the analyzed samples are reported in Table S1.

In Fig. 4 is reported as an example the Ti2p, Cu2p, and Ag3d spectra and the relative curve-fitting analysis for the sample TiCu-30%Ag (F). The measured BE value of the $Ti2p_{3/2}$ signal (458.7 eV) corresponds to the expected value for TiO_2 [34]: indeed, when exposed to air, Ti is always oxidized to titania in the outmost surface layer [35]. The $Cu2p_{3/2}$ signal results from two components peaks located at 933.0 eV and 935.0 eV that have been attributed to metallic (Cu) and oxidized (CuO) copper, respectively. Moreover, the presence of a shake-up satellite, evident in the spectrum at about 943.5 eV, is a distinctive feature of Cu in the +2 oxidation state [36]. Finally, the $Ag3d_{5/2}$ main peak position at 368.5 eV is typical of metallic Ag; a small higher BE component, about 10% of the main component peak, located at about 369.9 eV can also be observed in the spectrum, and can be attributed to oxidized, positively charged silver atoms, indicated as Ag_2O in Table S1 [37]. In all samples, Ti was completely oxidized to Ti(IV), Cu was partially oxidized to Cu(II), and most Ag was predominantly in the unoxidized metallic state, consistent with the different reactivity towards oxygen of the three metals (Table S1).

Preprints (www.preprints.org) | NOT PEER-REVIEWED | Posted: 24 June 2021 doi:10.20944/preprints202106.0601.v1

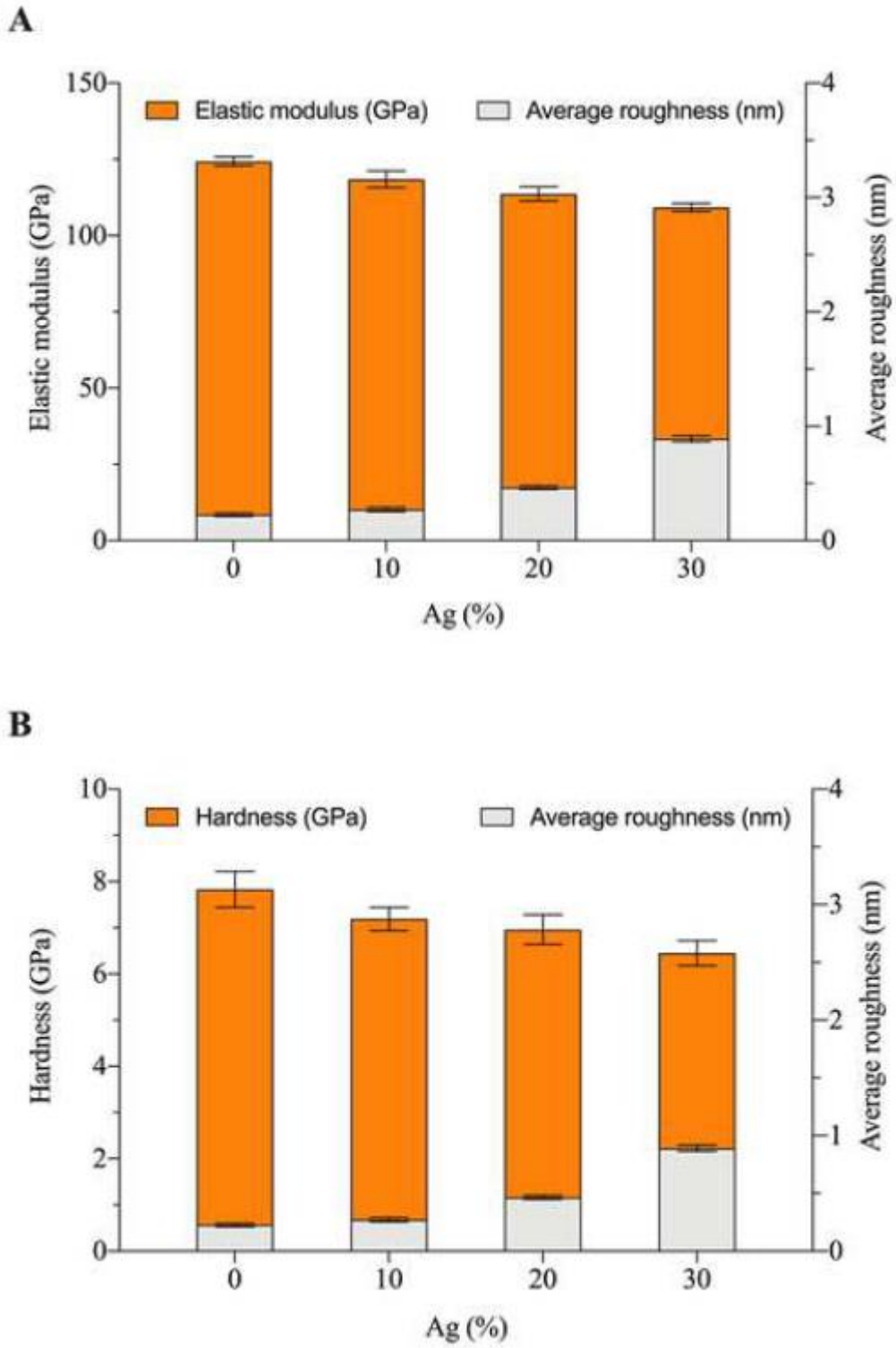

Figure 4. Comparison of elastic modulus and surface average roughness (A) and of hardness and surface average roughness (B) as a function of Ag content in TiCu thin films.

Preprints (www.preprints.org) | NOT PEER-REVIEWED | Posted: 24 June 2021 doi:10.20944/preprints202106.0601.v1

Peak areas have been used to calculate atomic ratios between the oxidized and metallic components and between the three elements present on the sample surface (Table S1). The measured atomic ratios between copper and titanium disagree with the expected value of 1:1, possibly because XPS is a surface-sensitive technique with a sampling depth of approximately ~5 nm. Therefore, the difference between measured and expected elemental composition is relative only to the outmost sample surface.

For TiCu samples, the copper concentration on the sample surface was lower than expected. On the other hand, the Ag:Ti atomic ratio on the surfaces of TiCu(Ag) thin films was higher than those of the targeted bulk values; a slight saturation effect has been observed at 30% Ag concentration. Apparently, when Ag was introduced in the mixture, Cu and Ag form an alloy and migrate together to the outmost sample surface, with Ag forming clusters as evidenced by AFM and XRD analysis (see Figures. 1 and 2).

We notice that the flaming procedure does not affect the sample surface composition and the oxidation state of the three elements.

3.2. Biocompatibility studies of the TiCu(Ag) surfaces

The TiCu(Ag) thin films biocompatibility has been evaluated by measuring human MRC-5 fibroblasts viability based on ATP production under aerobic conditions, which reflects the presence of metabolically active cells (Figure 5A). With this purpose, we first determined the correlation between the number of viable cells and the emitted luminescence (RLU) (Figure 5B). On the bases of the results obtained, we seeded 1.0×10^4 MRC-5 cells on polystyrene cell culture plate (Ctrl) and on sterile TiCu surfaces coated with 0%, 10%, 20%, and 30% Ag has been evaluated (Figure 5C). As shown, the number of cells after 24 h from seeding was comparable between Ctrl, TiCu, and TiCu(Ag) thin films, thus indicating that all the tested surfaces did not affect cell viability and proliferation.

Preprints (www.preprints.org) | NOT PEER-REVIEWED | Posted: 24 June 2021 doi:10.20944/preprints202106.0601.v1

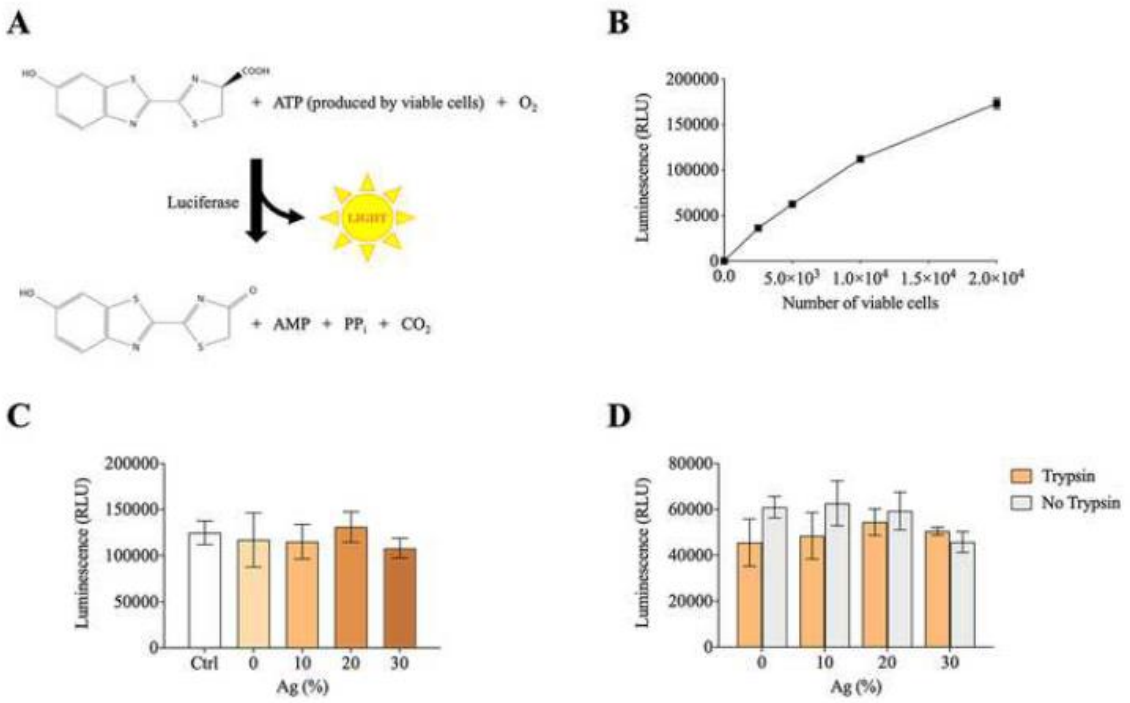

Figure 5. Evaluation of the biocompatibility of the TiCu and TiCu(Ag) surfaces. (A) Overview on the cell survival assay used to evaluate MRC5 cells grown on the TiCu surfaces. The CellTiter-Glo® reagent added to the cells generates a luminescent signal (relative light unit, RLU) that is proportional to the ATP present, which in turn is directly proportional to the number of metabolically active cells grown on the TiCu surface. (B) Set up of the assay sensitivity using MRC5 cells grown on TiCu surfaces. Cells were seeded in triplicate at a density of 2.5×10^3, 5.0×10^3, 1.0×10^4, 2.0×10^4, and 4.0×10^4 cells/well. (C) Cell viability assay measured 24 h after from seeding 1.0×10^4 MRC5 cells in triplicate on the 96-well plastic surface (Ctrl) or on the TiCu surfaces coated with 0%, 10%, 20%, and 30% Ag. (D) Cell viability assay measured after 24 h from seeding 1.0×10^4 MRC5 cells in triplicate on the TiCu surfaces coated with 0%, 10%, 20%, and 30% Ag, which were either previously treated with trypsin or not. Background luminescence was measured in well containing the medium without cells and subtracted from experimental values. Data are reported as means ± SD (Student's t test, $p<0.05$).

Preprints (www.preprints.org) | NOT PEER-REVIEWED | Posted: 24 June 2021 doi:10.20944/preprints202106.0601.v1

Next, in the perspective of using these surfaces for TE studies, we evaluated if the trypsin-mediated detachment of cells affected the biocompatibility of TiCu and TiCu(Ag) thin films. Results obtained indicated that trypsinization did not alter the capability of the TiCu(Ag) thin films to allow MRC-5 growth, supporting their possible use for tissue culture studies (Figure 5D).

3.3. XPS analysis of TiCu(Ag) surfaces after human MRC-5 cells trypsinization

To evaluate if thin film could be re-used for biocompatibility test after human cells detachment by trypsinization, TiCu(Ag) surfaces were analyzed by XPS and C1s, N1s, O1s, Ag3d, Ti2p and Cu2p core levels were investigated. XPS spectra and data (BE, FWHM, and atomic ratios) are reported in Figure 6 and Table S2. As already evidenced for the pristine samples, the Ti2p spectra are typical of TiO_2. The Cu2p spectra revealed the presence of both metallic and oxidized (CuO) copper, while the Ag3d signal is typical of metallic silver with a very small component related to oxidized silver (spectra not shown). No relevant change were evidenced on the oxidation state of metals on the sample surface. C1s, O1s and N1s spectra revealed the presence of organic molecules, particularly peptides, deposited on the TiCu(Ag) film surfaces.

Preprints (www.preprints.org) | NOT PEER-REVIEWED | Posted: 24 June 2021 doi:10.20944/preprints202106.0601.v1

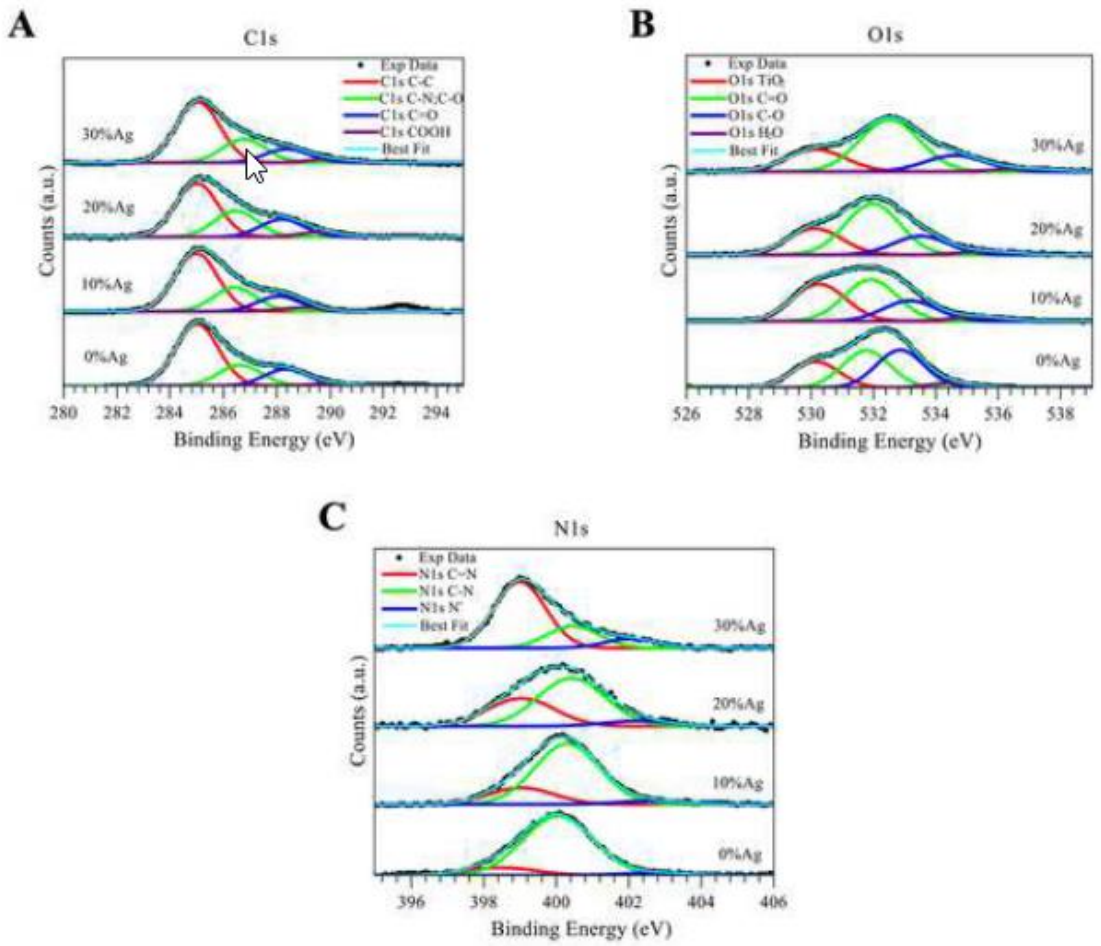

Figure 6. XPS spectra after human cells detachment by trypsinization. C1s (A), N1s (B) and O1s (C) XPS spectra of TiCu(Ag) films after human MRC-5 fibroblasts detachment with trypsin and related peak fitting analysis.

The curve fitting analysis of C1s core level spectra (Figure 6A) showed four components: (i) the peak at 285.0 eV indicating aliphatic C−C carbons; (ii) the peak at ~286.5 eV, related to C−N and C−O carbons of peptide backbones; (iii) the peak at 288.3 eV due to O=C−N peptide carbons; and (iv) the peak at 290.0 eV due to COOH carbons. The N1s spectrum (Figure 6B) comprised a peak at 399.0 eV due to C=N nitrogens, a main peak at 400.4 eV related to peptide nitrogens, and a peak at about 402.5 eV due to protonated nitrogens [32, 38]. The O1s spectra (Figure 6C) showed four component peaks: (i) the peak at 530.1 eV

Preprints (www.preprints.org) | NOT PEER-REVIEWED | Posted: 24 June 2021 doi:10.20944/preprints202106.0601.v1

assigned to the oxygens of titania; (ii) the peak at about 532.0 eV, assigned to O=C oxygens of the peptide backbone; (iii) the peak at 533.5 eV assigned to C-O oxygens; and (iv) the peak at nearly 535.0 eV, related to physiosorbed water [32].

In summary, the XPS data analysis points to the presence of peptide residues on the samples after human cells detachment, possibly representing cells residues of previous MRC-5 cell growth, not completely removed from the thin films by trypsin, and/or trypsin residues adsorbed on the sample surface. However, the presence of these peptode residues did not influence MRC-5 adhesion and proliferation, as reported in Figure 5D.

3.4. Evaluation of the bactericidal properties of the TiCu(Ag) surfaces

The bactericidal property of TiCu and TiCu(Ag) thin films was evaluated by testing the growth of two well-known nosocomial pathogens, *i.e. S. aureus* and *P. aeruginosa*. The experimental protocol is illustrated in Figure 7A. Briefly, *S. aureus* and *P. aeruginosa* were dispersed on either a glass surface or TiCu thin films coated with 0%, 10%, 20%, and 30% Ag. Bacteria were incubated for 24 h at 37°C in a controlled (99%) humidity chamber prior to mechanical detachment and cell (CFU) counting. For both species, limited or no loss of bacterial viability was observed on glass after 24 h (Figure 7B). Conversely, no colony growth was observed when bacteria were dispersed on TiCu and TiCu(Ag) surfaces, indicating a strong bactericidal activity (BA), even in the absence of Ag (Figure 7B). To evaluate the release of antibacterial agent(s) from the TiCu(Ag) surface, a suspension of *S. aureus* or *P. aeruginosa* was spread over NA plates, then TiCu(Ag) surfaces were placed onto the inoculated plates. The glass surface was used as the negative control (no growth inhibition), whereas antibiotic discs (*i.e.*, erythromycin, E 15 µg, and amikacin, AK/30 µg) were used as the positive control (growth inhibition due to antibiotic diffusion around the discs). No growth inhibition was observed around both glass and TiCu(Ag) surfaces, indicating no release of

Preprints (www.preprints.org) | NOT PEER-REVIEWED | Posted: 24 June 2021 doi:10.20944/preprints202106.0601.v1

inhibitory agent(s), as opposed to the large inhibition halo around the antibiotic discs (Figure 7C).

A

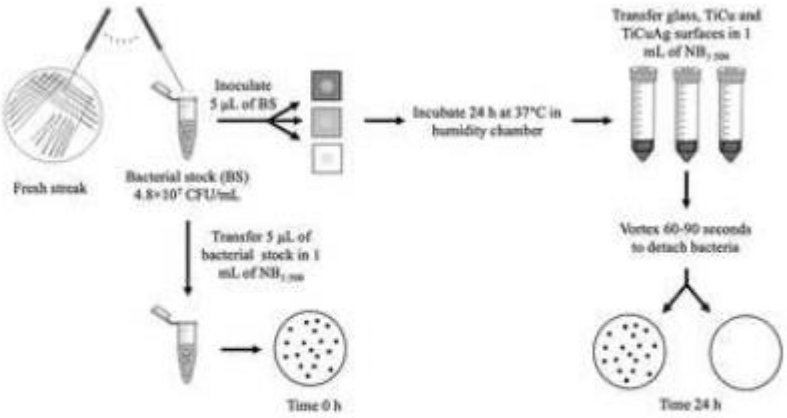

B

S. aureus

	0 h	24 h Glass	24 h TiCu	24 h TiCu-10% Ag	24 h TiCu-20% Ag	24 h TiCu-30% Ag
Number of colony forming unit (CFU)	201	163	0	0	0	0
	208	191	0	0	0	0
	212	223	0	0	0	0
Bactericidal activity (%)		–	100%	100%	100%	100%

P. aeruginosa

	0 h	24 h Glass	24 h TiCu	24 h TiCu-10% Ag	24 h TiCu-20% Ag	24 h TiCu-30% Ag
Number of colony forming unit (CFU)	49	53	0	0	0	0
	80	41	0	0	0	0
	113	247	0	0	0	0
Bactericidal activity (%)		–	100%	100%	100%	100%

C

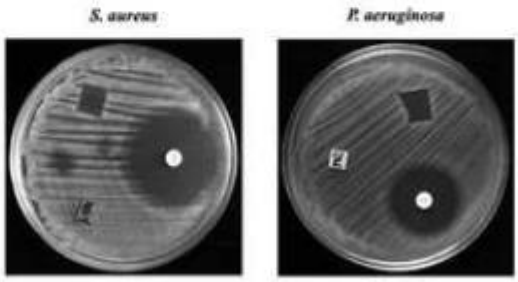

Figure 7. Bactericidal properties of the TiCu and TiCu(Ag) surfaces. (A) Schematic representation of the protocol used to test the bactericidal activity of the TiCu(Ag) surfaces.

Preprints (www.preprints.org) | NOT PEER-REVIEWED | Posted: 24 June 2021 doi:10.20944/preprints202106.0601.v1

(B) Bactericidal effect of TiCu(Ag) surfaces determined after 24h incubation at 37°C with 99% humidity of *S. aureus* and *P. aeruginosa* cells on TiCu(Ag) surfaces. The glass surface was used as negative control for bacterial killing. (C) Plate test for release of antibacterial agents from TiCu(Ag) urfaces. *S. aureus* and *P. aeruginosa* were used as test species. Antibiotic discs and glass were used as positive and negative controls of bacterial inhibition.

To exclude incomplete detachment of *S. aureus* and *P. aeruginosa* from $NB_{1:500}$-washed TiCu surfaces, both optical microscopy (Figure 8A) and AFM analyses (Figure 8B) were performed. Microscopy results were compared with positive control (Ctrl) samples in which the same number of bacteria was directly dispensed onto the TiCu surfaces, without subsequent washing step. A complete detachment of bacterial cells from TiCu surfaces was observed for both strains. Indeed, the large-scale optical microscopy images showed that on Ctrl samples many "coffee-stain" clusters were present (Figure 8A), while no clusters were observed on washed TiCu surfaces. This was confirmed by acquiring several images across the surfaces. By AFM characterization, the clusters on Ctrl samples were univocally identified as bacterial aggregates (Figure 8B). Notably, *S. aureus* bacteria showed a round shape, with an average diameter and height of 950 nm and 530 nm, respectively. The *P. aeruginosa* bacteria were instead shallower with an average height of 230 nm and showed an elongated shape, often with flagella, having an average long-axis length of 1300 nm. The tendency of bacteria towards clustering in Ctrl samples, evident in Figure 7B, was observed for similar deposition conditions and attributed to the capillary flow induced by the evaporation of the drop deposited [39, 40]. Conversely, the TiCu surfaces analyzed after bacteria detaching showed morphological features with heights below 30 nm (thus more than one order of magnitude lower than typical bacteria heights), likely to be attributed to residual of the nutrient medium used for the growth. The rms surface roughness evaluated on 20×20 μm^2 images was 1.71 nm and 1.87 nm after detachment of *S. aureus* and *P. aeruginosa*, respectively; while it

Preprints (www.preprints.org) | NOT PEER-REVIEWED | Posted: 24 June 2021 doi:10.20944/preprints202106.0601.v1

exceeded 50 nm for the Ctrl surfaces with bacteria adhered. This comparative morphological analysis confirms that: (*i*) bacteria were completely detached with the experimental protocol used for the plate-count experiments and, (ii) TiCu surfaces were bactericidal for both *S. aureus* and *P. aeruginosa*.

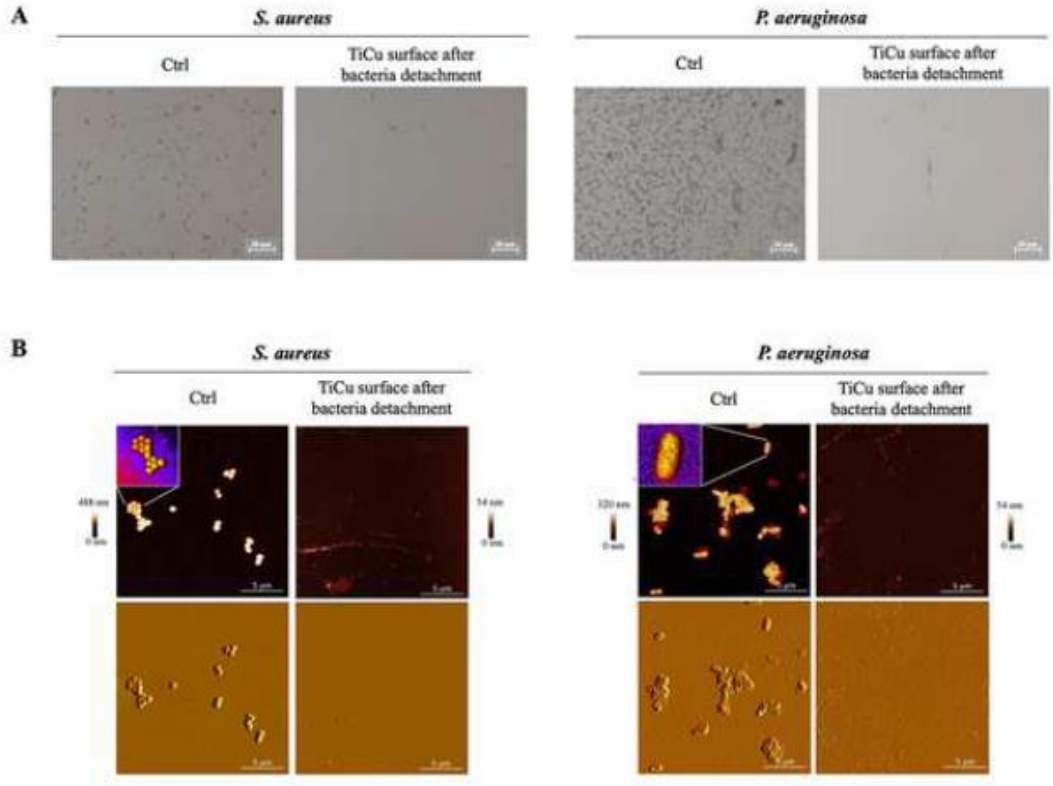

Figure 8. Surface morphology of TiCu samples after bacteria detachment. (A) Optical microscopy images and (B) AFM topographic (top panels) and peak-force error (bottom panels) images of control and TiCu surfaces on which *S. aureus* or *P. aeruginosa* were grown. Images were acquired after bacteria detaching and were compared to samples (Ctrl) where a suspension of each bacteria strain, containing the same number of bacteria as in the experiment, was poured directly on the TiCu surface. In the insets shown in panels B, 3D zoom ups are displayed.

4. Discussion

Preprints (www.preprints.org) | NOT PEER-REVIEWED | Posted: 24 June 2021 doi:10.20944/preprints202106.0601.v1

Here, the biocompatibility and the antibacterial properties of TiCu and TiCu(Ag) thin films, as produced by PVD magnetron sputtering method, are reported. All TiCu and TiCu(Ag) thin films display a good adhesion and growth of human fibroblast MRC5 cells, together with strong antibacterial activity against both *S. aureus* and *P. aeruginosa*, here considered as prototypes of nosocomial bacterial pathogens. Results are extremely significant for TE applications, biocompatibility and antibacterial performance representing key design parameters for biomaterials. In fact, tissue and implant-associated bacterial infection is a growing problem, responsible for increased morbidity and mortality, together with enormous economic losses to the public health system. Bacteria can tightly adhere to the biomaterial surface, and the formation of biofilm can help bacteria to escape the host immune system and antibiotics. In turn, this causes the emergence of bacterial resistance to antibacterial drugs and finally determines implantation failures [41]. Therefore, implanting materials that combine the capability to favor eukaryotic cells adhesion and proliferation for tissue regeneration with strong antibacterial properties are urgently needed. Metallic elements (*e.g.*, Au, Ag, Cu, and Zn) have been proven to exert antibacterial activity by surfaces coating or doping [42]. Remarkably, coating displays an amorphous single-phase structure with improved mechanical properties with respect to pure titanium up to Ag ~20%.

A main discussion point on the observed results should be the interpretation of surface chemical characterization of the films in relation with the observed functional properties. In fact, XPS analysis shows that TiO_2 represents the main oxidation state for titanium, thus explaining the observed biocompatibility. At the same time, all films show the presence of a combination between metallic and oxidized copper, with an increase of Cu/Ti ratio after addition of Ag. In addition, Ag is shown to be predominantly present in the metallic state with low levels of Ag_2O on the surface. Such observations can be used to explain the relevant antibacterial performance of the films. In fact, the presence of a single-phase film with

Preprints (www.preprints.org) | NOT PEER-REVIEWED | Posted: 24 June 2021 doi:10.20944/preprints202106.0601.v1

homogeneous surface distributions of Ag and Cu can be very effective in protecting the surface against bacteria, while maintaining a high biocompatibility thanks to the concurrent homogenous distribution of TiO_2.

The biocompatibility of TiCu(Ag) thin films here ported is in line with the very low cytotoxicity observed in Ag when tested in human blood, adenocarcinomic alveolar basal epithelial cells, liver cancer cells, breast cancer cells, and gastric cancer cells [43-45]. Noteworthy, several data support the anti-bacterial, anti-viral, anti-biofilm, and anti-inflammation activity of Ag, especially at nanoscale [43-47]. Furthermore, Cu is a transition metal and an essential micronutrient in humans and bacteria. Indeed, Cu is involved in many biosynthetic and metabolic processes, being a cofactor of many redox enzymes and playing a role in iron metabolism. In humans, Cu plays also an essential role in immune function [48]. It has been reported that TC_{50} values (*i.e.*, the value that indicates which is concentration of a specific substance that produces toxic effects in 50% of the cell population) for Cu is 344±4.4 μM in human gingival fibroblast [49], which means that it exerts a very low cytotoxicity. Besides, while low concentrations of Cu are essential for bacteria metabolism, high concentrations, cause cell growth inhibition or even cells death [50, 51]. Therefore, Cu represent an optimal metal to prepare antibacterial titanium alloys [42, 52, 53].

5. Conclusion

In this paper, the surface structural and functional properties of amorphous TiCu(Ag) thin film have been investigated. The increase of Ag content is accompanied by the appearance of Ag-nanocrystallites and by a decrease of both elastic modulus and hardness of the thin film. TiCu(Ag) thin films allowed a very good adhesion and growth of fibroblast MRC5 cells irrespective to different Ag content.

 doi:10.20944/preprints202106.0601.v1

Based on the multi-technique characterization and cellular studies, it can be concluded that binary TiCu and TiCu-10% Ag showed the best mechanical properties with amorphous glassy structure combined to excellent biocompatibility and antibacterial activity. On the contrary, ternary TiCu(Ag) thin films with 20% Ag content showed moderate mechanical properties, although they display excellent biocompatibility and antibacterial properties.

The excellent biocompatibility and bactericidal properties of these multifunctional thin films opens to their use in TE applications. Moreover, these types of thin films could be also used to coat surgical tools and hospital furnishing. For the future, it will be necessary to test these thin films for the biocompatibility of mesenchimal stem cells, one of the most studied stem cells for their great potential to enhance TE thanks to their capacity to differentiate into cartilage, bone, fat, muscle, tendon, skin as well as hematopoietic-supporting stroma and neural tissue [54]. Moreover, these kinds of thin films could be suitable for applications also against SARS-CoV-2 infection [20]. Indeed, Cu and its oxide have been demonstrated to act as efficient antiviral agents [20, 21, 55].

Funding

This work was supported by the grant “Piano straordinario di sviluppo della ricerca di Ateneo – Azione 4” from Roma Tre University to P. A. The Grant of Excellence Departments, MIUR (ARTICOLO 1, COMMI 314 – 337 LEGGE 232/2016) to the Department of Science, University Roma Tre is also gratefully acknowledged. Moreover, the Authors acknowledge the European Commission for support through the H2020 project OYSTER, g.a. n. 760827.

Acknowledgements

 doi:10.20944/preprints202106.0601.v1

Authors gratefully acknowledge the experimental support received form Dr. Giorgio Contini and Dr. Stefano Franchi in the XPS measurements, and Dr. Jacopo Albanesi for the validation of luminescence experiments.

References

[1] J.C. Dayoub, F. Cortese, A. Anžič, T. Grum, J.P. de Magalhães, The effects of donor age on organ transplants: A review and implications for aging research, Exp. Gerontol. 110 (2018) 230-240.

[2] http://www.transplant-observatory.org/

[3] B.M. Frey, S.M. Zeisberger, S.P. Hoerstrup SP, Tissue engineering and regenerative medicine - New initiatives for individual treatment offers, Transfus. Med. Hemother. 43 (2016) 318-319.

[4] C. Hennessy, G. Lewik, A. Cross, J. Hester, F. Issa, Recent advances in our understanding of the allograft response, Fac. Rev. 10 (2021) 21.

[5] S. Miyairi, W.M 3rd Baldwin, A. Valujskikh, R.L. Fairchild, Natural killer cells: critical effectors during antibody-mediated rejection of solid organ allografts, Transplantation 105 (2021) 284-290.

[6] M.J. Lysaght, J. Crager, Origins, Tissue Eng. Part A 15 (2009) 1449-1450.

[7] A.J. Salgado, J.M. Oliveira, A. Martins, F.G. Teixeira, N.A. Silva, N.M. Neve, N. Sousa, R.L. Reis, Tissue engineering and regenerative medicine: past, present, and future, Int Rev Neurobiol 108 (2013) 1-33.

[8] N. Ghosh, E.R. Banerjee, Nanoscaffolds in tissue engineering, in: E.R. Banerjee (Ed.), Nanomaterials and biomedicine, Springer, Singapore, 2020, pp. 57-66.

[9] F. Han, J. Wang, L. Ding, Y. Hu, W. Li, Z. Yuan, Q. Guo, C. Zhu, L. Yu, H. Wang, Z. Zhao, L. Jia, J. Li, Y. Yu, W. Zhang, G. Chu, S. Chen, B. Li, Tissue engineering and regenerative medicine: achievements, future, and sustainability in Asia, Front. Bioeng. Biotechnol. 8 (2020) 83.

[10] T. Lu, Y. Li Y, T. Chen, Techniques for fabrication and construction of three-dimensional scaffolds for tissue engineering, Int. J. Nanomedicine 8 (2013) 337-350.

[11] J.J. Swartjes, P.K. Sharma, T.G. van Kooten, H.C. van der Mei, M. Mahmoudi, H.J. Busscher, E.T. Rochford, Current developments in antimicrobial surface coatings for biomedical applications, Curr. Med. Chem. 22 (2015) 2116-2129.

[12] S. Korkmaz, İ.A. Kariper, Glass formation, production and superior properties of Zr-based thin film metallic glasses (TFMGs): a status review, J. Non Cryst. Solids 527 (2020) 119753.

[13] W. Wenbo, M. Hesham, D. Wahyu, P. C. Jinn, L. Lin, C. Wenjun, Effects of nanoscale chemical heterogeneity on the wear, corrosion, and tribocorrosion resistance of Zr-based thin film metallic glasses, Surf. Coat. Technol. 402 (2020) 126324.

[14] S. Ketov, X. Shi, G. Xie, G. Xie, R. Kumashiro, A. Y. Churyumov, A.I. Bazlov, N. Chen, Y. Ishikawa, N. sao, H. Wu, D.V. Louzguine-Luzgin, Nanostructured Zr-Pd metallic glass thin film for biochemical applications, Sci. Rep. 5 (2015) 7799.

[15] J.F. Correa, W. Aperador, J.C. Caicedo, N.C. Alba, C. Amaya, Structural, mechanical and tribological behavior of TiCN, CrAlN and BCN coatings in lubricated and non-lubricated environments in manufactured devices, Mater. Chem. Phys. 252 (2020) 123164.

[16] Mitsunori Yada, Yuko Inoue, Tomohiro Morita, Shintaro Imamura, Toshio Torikai, Takanori Watari, Synthesis and antibacterial activity of a silver nanoparticle/silver titanium phosphate–nanocomposite nanobelt thin film formed on a titanium plate, Thin Solid Films 628 (2017) 184-189.

[17] L. Somlyai-Sipos, P. Baumli, A. Sycheva, G. Kaptay, E. Szőri-Dorogházi, F. Kristály, T. Mikó, D. Janovszky, Development of Ag nanoparticles on the surface of Ti powders by chemical reduction method and investigation of their antibacterial properties, Appl. Surf. Sci. 533 (2020) 147494.

[18] B.C. Sousa, C.J. Massar, M.A. Gleason, D.L. Cote, On the emergence of antibacterial and antiviral copper cold spray coatings, J. Biol. Eng. 15 (2021) 8.

[19] J. Yang, H. Qin, Y. Chai, P. Zhang, Y. Chen, K. Yang, M. Qin, Y. Zhang, H. Xia, L. Ren, B. Yu, Molecular mechanisms of osteogenesis and antibacterial activity of Cu-bearing Ti alloy in a bone defect model with infection *in vivo*, J. Orthop. Translat. 27 (2021) 77-89.

[20] Z. Sun, K (Ken) Ostrikov, Future antiviral surfaces: Lessons from COVID-19 pandemic, Sustain. Mater. Techno. 25 (2020) e00203.

[21] M. Miyauchi, K. Sunada, K. Hashimoto, Antiviral effect of visible light-sensitive Cu_xO/TiO_2 photocatalyst, Catalysts 10 (2020) 1093.

[22] M. Janczarek, M. Endo, D. Zhang, K. Wang, E. Kowalska, Enhanced photocatalytic and antimicrobial performance of cuprous oxide/titania: the effect of titania matrix, Materials 11 (2018) 2069.

[23] H. Ji, M-C. Zhao, B. Xie, Y.-C. Zhao, D. Yin, C. Gao, C. Shuai, A, Atrens, Corrosion and antibacterial performance of novel selective-laser-melted (SLMed) Ti-xCu biomedical alloys, J. Alloys Compd. 864 (2021) 158415.

[24] W. Zhang, S. Zhang, H. Liu, L. Ren, Q. Wang, Y. Zhang, Effects of surface roughening on antibacterial and osteogenic properties of TiCu alloys with different Cu contents, J. Mater. Sci. Technol. 88 (2021) 158-167.

[25] W.C. Oliver, G.M. Pharr, An improved technique for determining hardness and elastic modulus using load and displacement sensing indentation experiments, J. Mater. Res. 7 (1992) 1564-1583.

[26] W.C. Oliver, G.M. Pharr, Measurement of hardness and elastic modulus by instrumented indentation: Advances in understanding and refinements to methodology. J. Mater. Res. 19 (2004) 3.

[27] https://www.iso.org/standard/54431.html

[28] D. Nečas, P. Klapetek, Gwyddion: an open-source software for SPM data analysis, Cent. Eur. J. Phys. 10 (2012) 181-188.

[29] A. Ewald, S.K. Glückermann, R. Thull, U. Gbureck, Antimicrobial titanium/silver PVD coatings on titanium, Biomed. Eng. Online 5 (2006) 22.

[30] A. Etiemble, C. Der Loughian, M. Apreutesei, C. Langlois, S. Cardinal, J.M. Pelletier, J.F. Pierson, P. Steyer, Innovative Zr-Cu-Ag thin film metallic glass deposed by magnetron PVD sputtering for antibacterial applications, J. Alloys Compd. 707 (2017) 155-161.

[31] D.Campoccia, L. Montanaro, C.R. Arciola, A review of the biomaterials technologies for infection-resistant surfaces. Biomaterials 34 (2013) 8533-8554.

[32] E. Dauvergne, C. Mullié, Brass alloys: copper-bottomed solutions against hospital-acquired infections, Antibiotics (Basel) 10 (2021) 286.

[33] S. Rashid, M. Sebastiani, M. Zeeshan Mughal, R. Daniel, E. Bemporad, Influence of the silver content on mechanical properties of TiCuAg thin films, Nanomaterials, 11 (2020): 435.

[34] J.F. Moulder, W.F. Stickle, P.E. Sobol, K.D. Bomben, Handbook of X-ray photoelectron spectroscopy, (J. Chastain, Ed.) Perkin-Elmer Corporation, Physical Electronics Division, Eden Prairie, Minnesota, 1992.

[35] S. Franchi, V. Secchi, M. Santi, M. Dettin, A. Zamuner, C. Battocchio, G. Iucci, Biofunctionalization of TiO_2 Surfaces with self assembling oligopeptides in different pH and ionic strength conditions: charge effects and molecular organization, Mater. Sci. Eng. C 90 (2018) 651-656.

[36] D.A. Svintsitskiy, T.Kardash, A.I. Boronin. Surface dynamics of mixed silver-copper oxide AgCuO2 during X-rayphotoelectron spectroscopy study, Appl. Surf. Sci 463 (2019) 300-309.

[37] I. Schiesaro, L. Burratti, C. Meneghini, I. Fratoddi, P. Prosposito, J. Lim, C. Scheu, C. Venditti, G. Iucci, C. Battocchio, Hydrophilic silver nanoparticles for Hg(II) detection in water: direct evidence for mercury-silver interaction, J. Phys. Chem. C 124 (2020) 25975-25983.

[38] G. Beamson, D Briggs, High resolution XPS of organic polymers: the Scienta ESCA 300 Database, J. Chem. Edu. 70 (1993) A25.

[39] D. Mampallil, H.B. Eral, A review on suppression and utilization of the coffee-ring effect, Adv. Colloid Interface Sci 252 (2018) 38-54.

[40] S. Bashiri, M. Lucidi, D. Visaggio, G. Capecchi, L. Persichetti, G. Cincotti, P. Visca, G. Capellini, Growth phase- and desiccation-dependent *Acinetobacter baumannii* morphology: an atomic force microscopy investigation, Langmuir 37 (2021) 1110-1119.

[41] C.R. Arciola, D. Campoccia, L. Montanaro, Implant infections: adhesion, biofilm formation and immune evasion, Nat. Rev. Microbiol. 16 (2018) 397-409.

[42] Z. Lin, X. Sun, H. Yang, The role of antibacterial metallic elements in simultaneously improving the corrosion resistance and antibacterial activity of magnesium alloys, Mater. Des. 198 (2021) 109350.

[43] B. Liu, Y.F. Zheng, Effects of alloying elements (Mn, Co, Al, W, Sn, B, C and S) on biodegradability and in vitro biocompatibility of pure iron. Acta Biomater. 7 (2011) 1407-1420.

[44] Y. Huang, X. Ding, Y. Qi, B. Yu, F.J. Xu. Reduction-responsive multifunctional hyperbranched polyaminoglycosides with excellent antibacterial activity, biocompatibility and gene transfection capability. Biomaterials 106 (2016) 134-144.

[45] K. Saravanakumar, R. Chelliah, D. MubarakAli, D.H. Oh, K. Kathiresan, M.H. Wang, Unveiling the potentials of biocompatible silver nanoparticles on human lung carcinoma A549 cells and *Helicobacter pylori*. Sci. Rep. 9 (2019) 5787.

[46] C.N. Lok, C.M. Ho, R. Chen, Q.Y. He, W.Y. Yu, H. Sun, P.K. Tam, J.F. Chiu, C.M. Che, Proteomic analysis of the mode of antibacterial action of silver nanoparticles, J. Proteome Res. 5 (2006) 916-924.

[47] O. Choi, Z. Hu, Size dependent and reactive oxygen species related nanosilver toxicity to nitrifying bacteria, Environ. Sci. Technol. 42 (2008) 4583-4588.

[48] J.Y. Uriu-Adams, C.L. Keen, Copper, oxidative stress, and human health, Mol. Aspects Med. 26 (2005) 268-298.

[49] Y. Issa, P. Brunton, C.M. Waters, D.C. Watts, Cytotoxicity of metal ions to human oligodendroglial cells and human gingival fibroblasts assessed by mitochondrial dehydrogenase activity, Dent. Mater. 24 (2008) 281-287.

[50] G. Faúndez, M. Troncoso, P. Navarrete, G. Figueroa, Antimicrobial activity of copper surfaces against suspensions of *Salmonella enterica* and *Campylobacter jejuni*, BMC Microbiol. 4 (2004) 19.

[51] L. Zhu, J. Elguindi, C. Rensing, S. Ravishankar, Antimicrobial activity of different copper alloy surfaces against copper resistant and sensitive *Salmonella enterica*, Food Microbiol. 30 (2012) 303-310.

[52] F. Heidenau, W. Mittelmeier, R. Detsch, M. Haenle, F. Stenzel, G. Ziegler, H. Gollwitzer, A novel antibacterial titania coating: metal ion toxicity and in vitro surface colonization, J. Mater. Sci. Mater. Med. 16 (2005) 883-888.

[53] E. Zhang, F. Li, H. Wang, J. Liu, C. Wang, M. Li, K. Yang, A new antibacterial titanium-copper sintered alloy: preparation and antibacterial property, Mater. Sci. Eng. C Mater. Biol. Appl. 33 (2013) 4280-4287.

 doi:10.20944/preprints202106.0601.v1

[54] A.J. Rosenbaum, D.A Grande, J.S. Dines, The use of mesenchymal stem cells in tissue engineering: a global assessment, Organogenesis 4 (2008) 23-27.

[55] N. Hutasoit, B. Kennedy, S. Hamilton, A. Luttick, R.A.R. Rashid, S. Palanisamy, Sars-CoV-2 (COVID-19) inactivation capability of copper-coated touch surface fabricated by cold-spray technology, Manuf. Lett 25 (2020) 93-97.